International Journal of Current Science Research and Review
ISSN: 2581-8341
Volume 08 Issue 06 June 2025
DOI: 10.47191/ijcsrr/V8-i6-29, Impact Factor: 8.048
IJCSRR @ 2025
www.ijcsrr.org

# Conversion of Waste Cooking Oil into Biofuel through $CeO_2$-Based Oxide Catalysts ($CeO_2$-$La_2O_3$-NiO)

**Afifah Rosyidah[1,2*], Radhila Widya Putri Octora[1]**
[1]Materials and Energy Laboratory, Department of Chemistry, Faculty of Science and Data Analytics, Institut Teknologi Sepuluh Nopember (ITS), Sukolilo, Surabaya 60111, East Java, Indonesia
[2]Energy and Environment Laboratory, Institut Teknologi Sepuluh Nopember (ITS), 5th Floor Research Center Building, Sukollilo, Surabaya 60111, East Java, Indonesia

**ABSTRACT:** The $CeO_2$-based oxide catalysts ($CeO_2$-$La_2O_3$-NiO) were successfully synthesized with different concentrations of microcrystalline cellulose (MCC). The resulting materials underwent characterization through various techniques, including TGA, XRD, FTIR, TEM, FESEM-EDX, and $N_2$ adsorption-desorption. XRD characterization revealed that the $CeO_2$ phase was a stable compound in all synthesized products. The semi-batch reactor was operated for 4 hours at 360 °C for the deoxidation reaction of used cooking oil using 1 wt% product catalyst. Deoxygenation occurred perfectly in the sample using BCOe-12.5 wt% MCC catalyst, resulting in 99% hydrocarbon selectivity and yielding 46% liquid product. These findings underscore the effectiveness of $CeO_2$-based oxides ($CeO_2$-$La_2O_3$-NiO) as promising catalysts for biofuel synthesis.

**KEYWORDS:** Biofuel, $CeO_2$-*Based Oxide* ($CeO_2$-$La_2O_3$-NiO), Deoxygenation, Microcrystalline Cellulose, Waste Cooking Oil

## 1. INTRODUCTION

Over the past century, the Earth's surface temperature has risen by roughly 0.8 °C, alongside a sea level increase of approximately 18 cm. This warming trend is strongly associated with excessive carbon emissions resulting from fossil fuel combustion(Xu M, et al., 2024). Although renewable energy has experienced significant development, fossil fuels remain the dominant energy source globally, accounting for about 80% of total use(Bian Z, et al., 2020). This continued dependence has encouraged the use of alternative energy as a solution(Adedoyin FF, et al., 2021), among which biomass energy; such as biofuels, biogas, used cooking oil, microalgae oil, ammonia fuel, and hydrogen produced from renewable energy, microalgae oil, and animal fats, stand out as promising candidates for producing carbon-neutral fuels(Tsiotsias AI, et al., 2023).

In the past eight years, global waste cooking oil production has surged by 16.6 million tons, marking a 79% increase(Loizides MI, et al., 2019). Typically, waste cooking oil contains over 90% triglycerides(Hosseinzadeh-Bandbafha H, et al., 2021). However, improper disposal can lead to severe environmental hazards. Repurposing waste cooking oil into valuable products offers a sustainable approach to reducing its negative environmental impact while simultaneously fostering the growth of a bioeconomy centered on waste-derived fuel. Due to its widespread availability, affordability, and potential to be refined into eco-friendly liquid fuels, waste cooking oil presents a viable renewable energy solution that addresses both waste management and rising energy demands(Adedoyin FF, et al., 2021).

Used cooking oil has unstable physicochemical properties, such as high viscosity and low calorific value; making it unsuitable for direct use as fuel. This problem negatively impacts the quality of the fuel due to the presence of carboxyl groups which are oxidized compounds. The main approach to converting used cooking oil into viable biofuel is the catalytic deoxygenation process. This approach targets the cleavage of the C-O bond chains in the oxidized compounds, thereby enhancing the biofuel components while improving overall fuel efficiency(Tsiotsias AI, et al., 2023; Pham LKH, et al., 2018).

The success of this process is highly dependent on the catalyst used, as it enhances the reaction efficiency and promotes deoxygenation. Among the various catalysts available, oxide-based materials have shown strong catalytic activity. In particular, this occurs in Cerium oxide ($CeO_2$). This oxide catalyst is very suitable because it has excellent ability to attract, store, and release oxygen. This condition is supported by the occurrence of a reversible oxidation-reduction process from the transition state involving $Ce^{3+}$ and $Ce^{4+}$. This makes $CeO_2$ very suitable for catalytic applications, including energy storage. In addition, Lanthanum oxide ($La_2O_3$) is also an integral part of the process that is able to promote the decarboxylation mechanism. It is very efficient in breaking

International Journal of Current Science Research and Review
ISSN: 2581-8341
Volume 08 Issue 06 June 2025
DOI: 10.47191/ijcsrr/V8-i6-29, Impact Factor: 8.048
IJCSRR @ 2025
www.ijcsrr.org

the C-O bond and producing other hydrocarbon bonds in the position range at C15–C17. This condition is very suitable for use as fuels(Ruan Y, et al., 2020). Nickel as a catalyst base, highly appreciated due to its very reasonable cost, provides enhanced deoxygenation effects comparable to noble metal catalysts, as evidenced by numerous studies emphasizing its contribution to biofuel synthesis. The synergy of these mixed oxides offers an effective approach to enhance biofuel production by facilitating the deoxygenation of waste cooking oil with high catalytic efficiency(Sagar T V, et al., 2020).

However, metal oxide-based catalysts naturally possess limited pore sizes and surface areas (Ooi XY, et al., 2019), which can restrict their overall performance. To address this limitation, template incorporation is essential for enhancing their physicochemical properties. The process of using synthetic templates often causes environmental problems and is expensive, thus limiting its use for large-scale industrial applications. Recent studies have shown that ZSM-5 material was successfully synthesized by utilizing microcrystalline cellulose (MCC) as a natural template, which significantly improves the pore structure and surface area, thus offering a more sustainable approach for catalyst development(Li X, et al., 2023; Qian M, et al., 2020).

Building on recent advancements, this study explores the application of biomass-derived microcrystalline cellulose (MCC) as a templating agent in the synthesis of $CeO_2$-based oxides ($CeO_2$-$La_2O_3$-NiO) to improve pore structure and surface characteristics. Various mixed metal oxides will be synthesized at different calcination temperatures and assessed to identify the optimal composition that enhances catalytic performance during the deoxygenation of waste cooking oil. The primary objective of this research is to develop biofuel with a high liquid yield and superior hydrocarbon selectivity, contributing to a more sustainable and efficient approach to future energy demands.

## 2. MATERIAL AND METHODS

### 2.1 Material

The study utilized several materials, including MCC cellulose as microcrystalline, lanthanum(III) nitrate hexahydrate ($La(NO_3)_3 \cdot 6H_2O$) with 99% purity produced by Sigma Aldrich, cerium(III) nitrate hexahydrate ($Ce(NO_3)_3 \cdot 6H_2O$) with 99% purity produced by Sigma Aldrich, and nickel (II) nitrate hexahydrate ($Ni(NO_3)_2 \cdot 6H_2O$) with 99% purity from Sigma Aldrich. Additionally, ethanol ($C_2H_5OH$) with 96% purity from Merck, citric acid (Sigma Aldrich, 99%), deionized water, and waste cooking oil were employed in the experimental procedures.

### 2.2 Instrumentation

The experimental setup for this study is divided into two main categories: equipment for synthesizing $CeO_2$-based oxide catalysts ($CeO_2$-$La_2O_3$-NiO) and instruments for characterizing the resulting solid samples. The synthesis apparatus includes an analytical balance, watch glass, beaker glass, spatula, measuring cylinder, Duran bottles, magnetic stirrer, hot plate, ceramic crucible, oven, muffle furnace, mortar, and pestle. Meanwhile, the characterization instruments consist of TGA Thermogravimetric Analysis Hitachi STA7200 Simultaneous Thermal Analyzer, XRD X-ray Diffraction X'PertPRO PANalytical, FTIR Fourier Transform Infrared Shimadzu Instrument Spectrum One 8400S, Transmission Electron Microscopy (TEM) Hitachi type HR-9500 TEM, Field Emission Scanning Electron Microscopy (FESEM) and Energy Dispersive X-ray Spectroscopy (EDX) produced by Hitachi S4800, Nitrogen Adsorption-Desorption Analysis, and GC-MS Gas Chromatography–Mass Spectrometry Analysis.

### 2.3 Procedure

2.3.1 Preparation of Microcrystalline Cellulose (MCC)

To prepare microcrystalline cellulose (MCC), 26 g of the material was weighed and transferred into a beaker, then 260 mL of distilled water was added, and the mixture underwent ultrasonication for 1 hour to ensure dispersion.

2.3.2 Synthesis of $CeO_2$ -Based Oxide Catalysts ($CeO_2$-$La_2O_3$-NiO)

The synthesis of $CeO_2$-based oxide catalysts ($CeO_2$-$La_2O_3$-NiO) was carried out using an in-situ method, modified from Ruan et al., 2020b, incorporating adjustments in the hard template and metal precursors. This process involves a citric acid solution to which $La(NO_3)_3 \cdot 6H_2O$, $Ce(NO_3)_3 \cdot 6H_2O$, $Ni(NO_3)_2 \cdot 6H_2O$, in a stoichiometric ratio is added, followed by the addition of 10 mL of deionized water and 30 mL of ethanol. The resulting solution was stirred continuously at room temperature for 12 hours to ensure uniformity. After this, microcrystalline cellulose was added at various concentrations and the mixture was homogenized again for another 24 hours at 60 °C. The resulting solution, formed into a hard mold, was then evaporated using a hot plate at 80 °C. The

International Journal of Current Science Research and Review
ISSN: 2581-8341
Volume 08 Issue 06 June 2025
DOI: 10.47191/ijcsrr/V8-i6-29, Impact Factor: 8.048
IJCSRR @ 2025
www.ijcsrr.org

resulting gel was then dried using an oven for 24 hours at a constant temperature of 70 °C, followed by a calcination process for 4 hours at 300 °C using a muffle furnace. The synthesized catalysts were labeled BOCe, BOCe-12.5%, BOCe-25%, and BOCe-37.5%.

**2.3.3 Material Characterization**

1) TGA *Thermogravimetric Analysis*

To determine the optimal calcination temperature and to remove the hard mold from the prepared sample, Thermogravimetric Analysis was used. The results of the analysis are the curve of the rate of loss of % mass against temperature variations. A total of 100 mg of the calcined sample was placed in an $Al_2O_3$ container and heated gradually from 0 to 1100 °C at a rate of 15 °C/min under air atmospheric conditions. The results were recorded as a mass loss curve (% weight loss) corresponding to temperature variations.

2) *X-ray Diffraction* (XRD)

XRD characterization was conducted to identify the crystal structure and phase composition of the synthesized materials. This analysis utilized an X-ray Diffractometer equipped with monochromatic Cu Kα radiation (λ = 1.5406 Å), operated at 40 kV voltage and 30 mA current. Scanning was performed over a 2θ range of 1–80°, with diffraction patterns compared against Joint Committee on Powder Diffraction Standards reference cards. Additionally, the Debye-Scherrer equation was used to predict the crystallite size

3) *Fourier Transform Infrared* (FTIR)

To analyze the functional groups contained in the solid samples resulting from synthesis in the wave number range of 4000–400 $cm^{-1}$, Fourier Transform Infrared was used. Each sample was mixed with KBr (acting as a dispersing agent) at a ratio of 1-2:99-98, ensuring a homogeneous blend. The mixture was finely ground, compressed into pellets using a hydraulic press, placed into the spectrometer's sample holder, and scanned utilizing an infrared spectrophotometer.

4) *Transmission Electron Microscopy* (TEM)

TEM characterization was conducted to analyze the pore structure, microstructure, and atomic configuration of the synthesized materials. Observations were performed at magnifications ranging from 50,000 to 600,000 times. Before imaging, the specimens were uniformly distributed in isopropyl alcohol to ensure optimal dispersion and carefully transferred onto a TEM grid for further examination.

5) *Field Emission Scanning Electron Microscopy and Energy Dispersive X-ray Spectroscopy* (FESEM-EDX)

Evaluation of the surface morphology and elemental composition of the synthesized samples was analyzed using FESEM-EDX. The solid samples were affixed onto carbon tape, followed by a Pd/Au coating process for 15 minutes at a pressure of $6 \times 10^{-2}$ mBar. Once the coating was completed, the specimens were transferred to the sample chamber for structural assessment.

6) $N_2$ Adsorption-Desorption Analysis

To investigate surface characteristics, nitrogen adsorption-desorption isotherm analysis was carried out by weighing 0.2 g of the material, followed by vacuum treatment at 300 °C for 3 hours and nitrogen gas purging at 350 °C. The Brunauer-Emmett-Teller (BET) equation was used to determine the specific surface area, while the Barrett-Joyner-Halenda (BJH) method was used to determine the pore size distribution. In addition, a t-plot approach is needed to determine the pore volume.

**2.4 Evaluation of Catalytic Performance in Waste Cooking Oil Deoxygenation**

The semi-batch reactor used in the used cooking oil deoxygenation process is equipped with a magnetic stirrer and a heating mantle. A catalyst comprising 1 wt% was added to 10 g of waste cooking oil within a three-neck flask reactor. The mixture underwent stirring and heating to a reaction temperature of 360 °C for 4 hours. The resulting liquid product obtained from the reaction was gathered in a condensation chamber kept at 18 °C, ensuring an efficient condensation process. Gas Chromatography-Mass Spectrometry (GC-MS) was used for comprehensive analysis of the end products of the deoxygenation process.

International Journal of Current Science Research and Review
ISSN: 2581-8341
Volume 08 Issue 06 June 2025
DOI: 10.47191/ijcsrr/V8-i6-29, Impact Factor: 8.048
IJCSRR @ 2025
www.ijcsrr.org

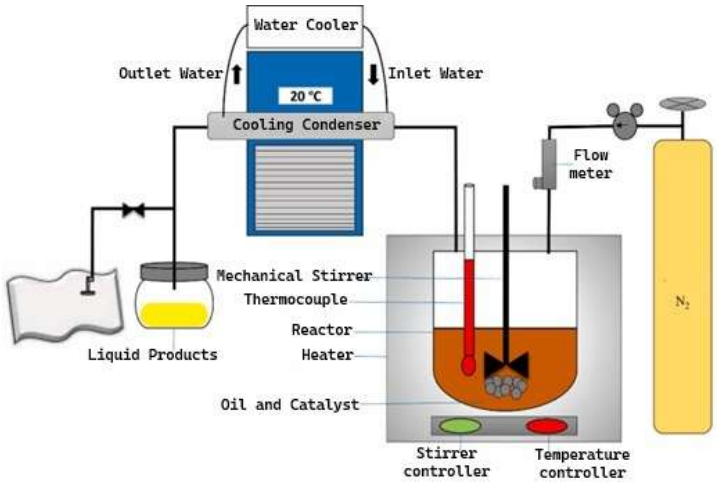


**Figure 1: Deoxygenation reactor for biofuel production**

### 2.5 *Gas Chromatography-Mass Spectrometry* (GC-MS)

The gas chromatography-mass spectrometry (GC-MS) was employed to identify the components within the liquid products generated from the reaction. The Shimadzu QP 2010 SE instrument, equipped with both FID and MS detectors, was utilized for this analysis. Two columns were used: the Rtx-5MS column containing 95% dimethyl polysiloxane and 5% diphenyl; and also the Carbowax column composed of polyethylene glycol. Helium served as the carrier gas during the analytical process. The GC-MS data interpretation involved the application of these formulas:

$$\text{Conversion (\%)} = \frac{\text{Initial reactant mass (g) - Final reactant mass (g)}}{\text{Initial reactant mass (g)}} \text{ x } 100\% \quad (2.1)$$

$$\text{Liquid Product Yield} = \frac{\text{Liquid product mass}}{\text{Reactant mass}} \text{ x } 100\% \quad (2.2)$$

$$\text{Diesel Selectivity (\%)} = \frac{\text{Hydrocarbon Fraction (C15-C17)}}{\text{Total Hydrocarbon Area (C8-C20)}} \text{ x } 100\% \quad (2.3)$$

## 3. RESULTS AND DISCUSSION

### 3.1 Synthesis of $CeO_2$-Based Oxide Catalyst ($CeO_2$-$La_2O_3$-NiO)

The synthesis began by dissolving citric acid, $La(NO_3)_3 \cdot 6H_2O$, $Ce(NO_3)_3 \cdot 6H_2O$, and $Ni(NO_3)_2 \cdot 6H_2O$ in a stoichiometric ratio in 10 mL of deionized water and 30 mL of ethanol. The products displayed a sage-green color due to the presence of nickel. The mixture was continuously agitated at ambient temperature for 12 hours to ensure complete uniformity. Following this, the well-mixed solution underwent a drying process on a hotplate set to 80°C, facilitating solvent evaporation and solid formation, forming a gel due to the presence of microcrystalline cellulose. This gel was subsequently oven-dried at 70°C, producing a solid foam-like sample with a sage-green hue. The solid foam was ground into a fine powder before undergoing calcination at 300°C for 4 hours in a muffle furnace. This calcination process significantly influenced the final textural properties of the $CeO_2$-based oxide material ($CeO_2$-$La_2O_3$-NiO).

International Journal of Current Science Research and Review
ISSN: 2581-8341
Volume 08 Issue 06 June 2025
DOI: 10.47191/ijcsrr/V8-i6-29, Impact Factor: 8.048
IJCSRR @ 2025
www.ijcsrr.org

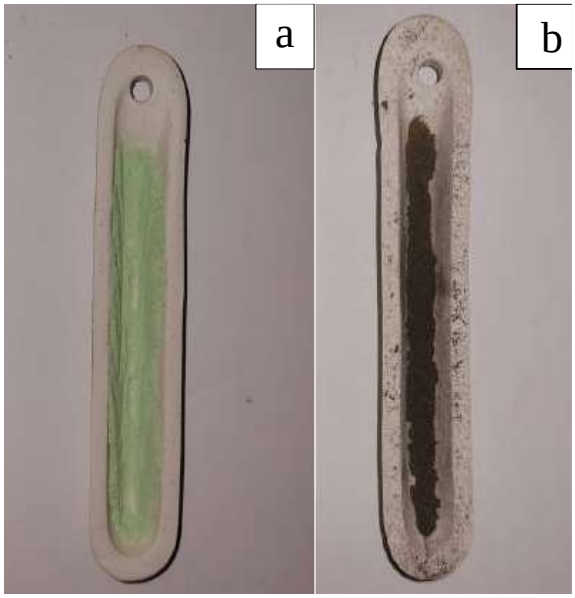


**Figure 2: $CeO_2$-Based Oxide Catalyst ($CeO_2$-$La_2O_3$-NiO) a) Before Calcination and b) After Calcination**

### 3.2 3.2 Characterization of $CeO_2$-Based Oxide Catalysts ($CeO_2$-$La_2O_3$-NiO)

3.2.1 *Thermal Gravimetric Analysis* (TGA)

TGA was utilized to evaluate the thermal stability and decomposition behavior of the samples. The analysis was performed across a temperature range from room temperature to 1000 °C, capturing data on heat flow, weight loss, and rate of weight reduction. As illustrated in Figure 3, the decomposition profiles differ depending on MCC content:

- Samples containing 12.5% and 37.5% MCC undergo three distinct decomposition stages, which include the elimination of physical and crystalline water, the breakdown of nitrates, and the decomposition of citric acid, followed by phase transitions at elevated temperatures.
- Conversely, the sample with 25% MCC content exhibits only two decomposition stages.

For all samples, initial weight reduction occurs within the 50-200 °C range, characterized by an endothermic peak. The most significant weight reduction between 200-400 °C is associated with an exothermic reaction, stemming from nitrate decomposition that releases NOx and oxygen gases. Furthermore, an exothermic reaction occurs between 400-600 °C, linked to oxide formation. Phase development is finally observed between 600-800 °C(Çoban Özkan D, et al., 2020).

International Journal of Current Science Research and Review
ISSN: 2581-8341
Volume 08 Issue 06 June 2025
DOI: 10.47191/ijcsrr/V8-i6-29, Impact Factor: 8.048
IJCSRR @ 2025
www.ijcsrr.org

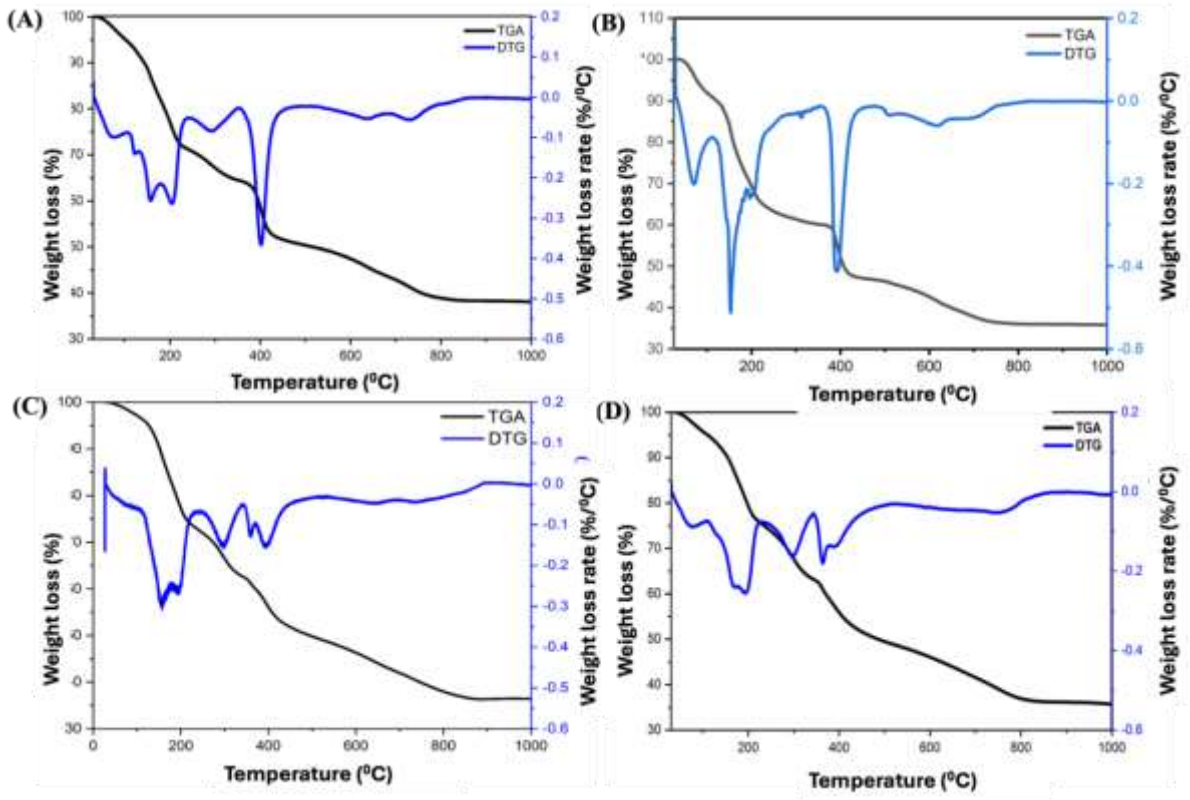


**Figure 3: a) BOCe, b) BOCe-12,5wt% MCC, c) BOCe-25wt% MCC, and d) BOCe-37,5wt% MCC**

3.2.2 *X-ray Diffraction* (XRD)

The XRD diffractogram patterns of $CeO_2$-based oxide catalysts ($CeO_2$-$La_2O_3$-NiO) with various concentrations of microcrystalline cellulose (MCC) are shown in Figure 4. As per JCPDS No. 34-0934, the XRD patterns of all the analyzed samples show distinct diffraction peaks associated with $CeO_2$, at diffraction angles (2θ) of 55.28°, 46.64°, 32.31°, and 27.81°, respectively, which correspond to the (3 1 1), (2 2 0), (2 0 0), and (1 1 1) crystallographic planes of the cubic framework of $CeO_2$. These observations confirm the successful development of stable and well-defined cubic phase of $CeO_2$ in all the tested materials(Wang L, et al., 2023). Although the addition of MCC as a template did not change the phase structure of $CeO_2$, there was a decrease in the intensity of the diffractogram peaks with increasing MCC content. The increase in MCC content also indicated an increase in the dispersion of $CeO_2$ crystallites and an increase in the proportion of amorphous phase due to the integration of MCC. For the sample with 37.5% MCC, the diffraction peaks appeared broader than those of the sample containing 12.5% MCC, which implied a smaller crystallite size or greater structural disorder.

The XRD patterns of the samples did not reveal any diffraction peaks corresponding to $La_2O_3$ and NiO, suggesting that Ni and La were partially substituted into the $CeO_2$ crystal lattice during synthesis. This substitution occurred due to the ionic size compatibility of $Ni^{2+}$ and $La^{3+}$ with the cubic $CeO_2$ structure. Consequently, $La_2O_3$ and NiO oxide phases did not form. Additionally, the Ni and La content in the samples was very low, causing their peak intensities to fall below the detection limit of XRD. The XRD method has limitations in detecting minor phases with extremely low concentrations, especially if their peak intensities overlap with $CeO_2$ peaks or are within a low signal-to-noise ratio.

International Journal of Current Science Research and Review
ISSN: 2581-8341
Volume 08 Issue 06 June 2025
DOI: 10.47191/ijcsrr/V8-i6-29, Impact Factor: 8.048
IJCSRR @ 2025
www.ijcsrr.org

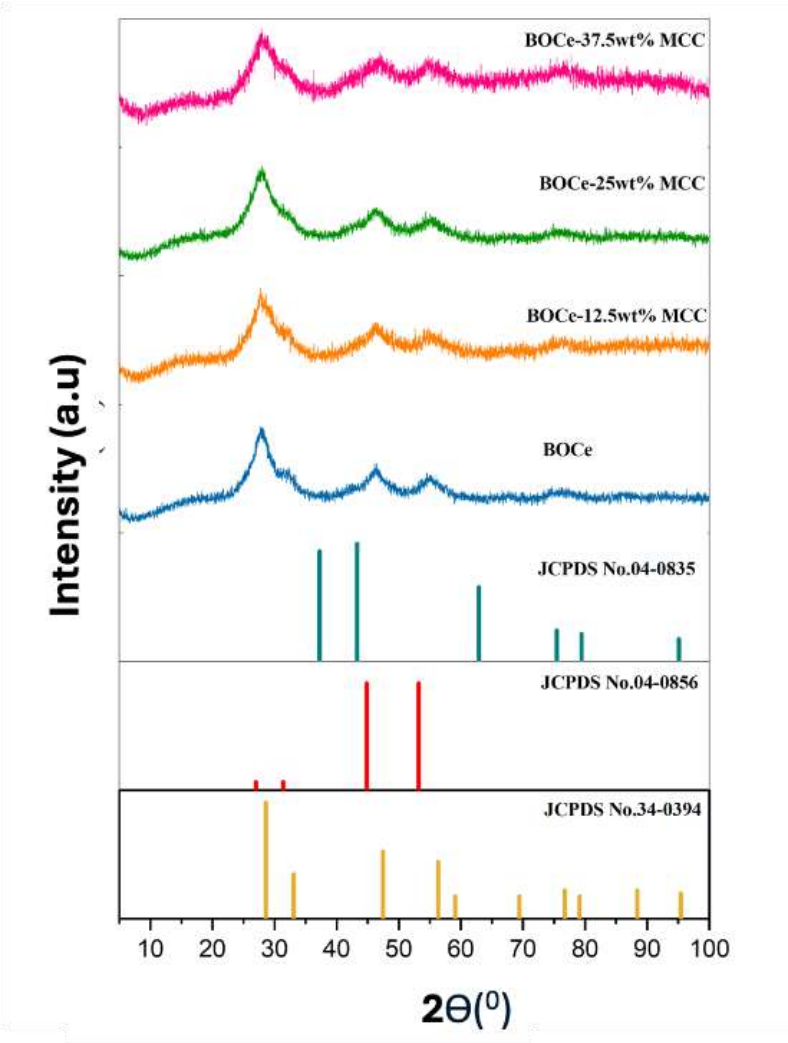


**Figure 4: XRD patterns of $CeO_2$-based oxide catalysts ($CeO_2$-$La_2O_3$-NiO)**

3.2.3 *Fourier Transform Infrared* (FTIR)

The FTIR spectroscopy analysis method provides information regarding functional groups, compound identification, and material mixture analysis in the sample. The FTIR vibration spectra of $CeO_2$-based oxide catalysts ($CeO_2$-$La_2O_3$-NiO) after calcination are shown in Figure 5. Absorption peaks were detected at wavenumbers 3445, 1484, 1382, 1064, dan 853 $cm^{-1}$. The broad absorption peak around 3445 $cm^{-1}$ is associated with O–H stretching vibrations, indicating the presence of adsorbed water or hydroxyl groups[15 Z, et al., 2020)]. The presence of hydroxyl groups can contribute to catalytic properties through interactions with reactant molecules. Peaks around 1484 $cm^{-1}$ and 1382 $cm^{-1}$ correspond to carbonate ($CO_3^{2-}$), vibrations, likely resulting from $CO_2$ adsorption on the material surface during calcination or exposure to air. Additionally, peaks at 853 $cm^{-1}$ and 1064 $cm^{-1}$ indicate C–O bending vibrations and C–O stretching, respectively, which may stem from residual carbonate or organic compounds remaining after calcination (Ruan Y, et al., 2020).

International Journal of Current Science Research and Review
ISSN: 2581-8341
Volume 08 Issue 06 June 2025
DOI: 10.47191/ijcsrr/V8-i6-29, Impact Factor: 8.048
IJCSRR @ 2025
www.ijcsrr.org

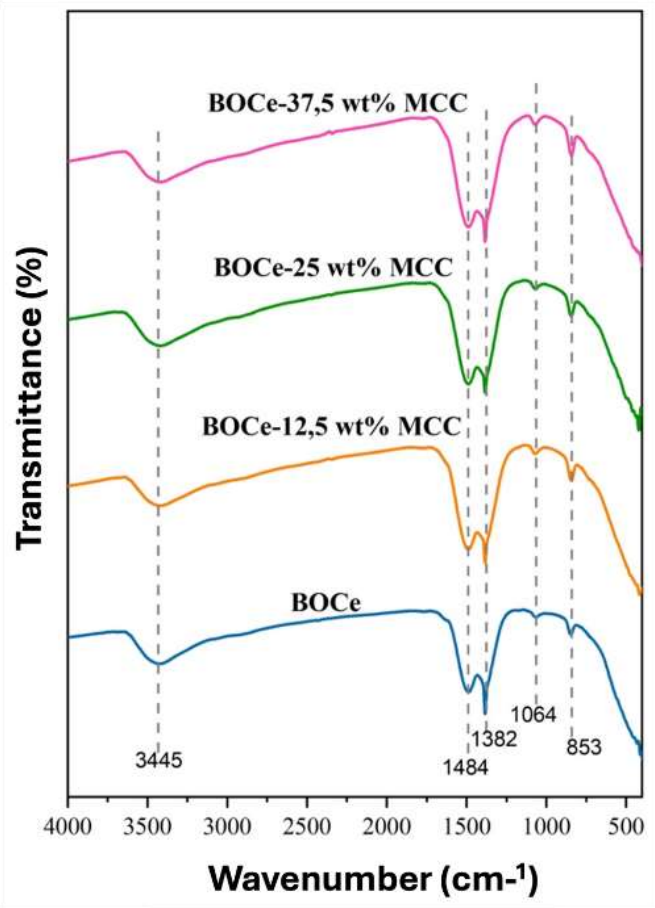


**Figure 5: FTIR spectra of $CeO_2$-based oxide catalysts ($CeO_2$-$La_2O_3$-NiO) after calcination**

3.2.4 *Transmission Electron Microscopy* (TEM)

Figure 6 illustrates the TEM images of the BOCe sample, taken at 20 nm magnification, revealing particle clustering and agglomeration. This behavior is attributed to the presence of organic compounds, such as citric acid, employed during synthesis.

At 5 nm magnification, the TEM image displays the interplanar spacing (d-spacing) of $CeO_2$, measured at 0.197 nm, which corresponds to the (1 1 1) crystal plane index. This observation is consistent with findings documented by Zhang L, et al., 2015

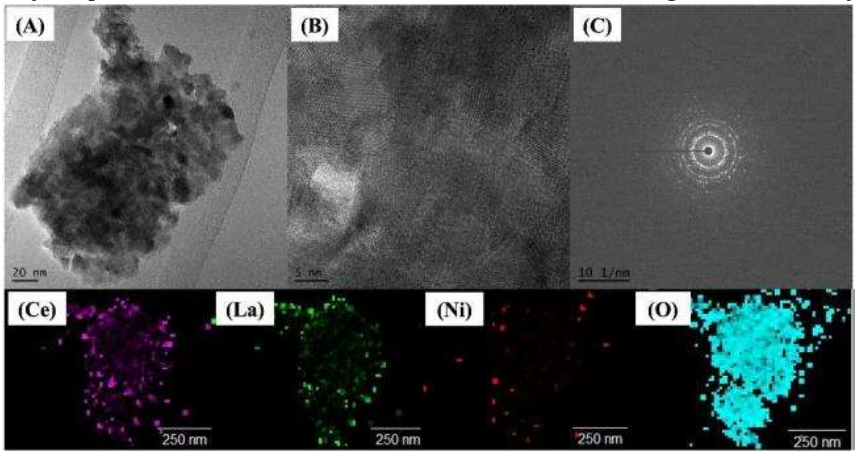


**Figure 6: TEM Micrographs of BOCe**

International Journal of Current Science Research and Review
ISSN: 2581-8341
Volume 08 Issue 06 June 2025
DOI: 10.47191/ijcsrr/V8-i6-29, Impact Factor: 8.048
IJCSRR @ 2025
www.ijcsrr.org

3.2.5 *Field Emission Scanning Electron Microscopy* (FESEM-EDX)

The structural and surface morphological features of the synthesized materials were characterized using *Field Emission Scanning Electron Microscopy* (FE-SEM). Observations conducted at a magnification scale of up to 1 µm revealed sponge-like particles with distinct pore structures in all samples structures(Barbosa KKF, et al., 2024). As shown in Figure 7a, the BOCe sample without MCC exhibited large, irregular pores, likely caused by the breakdown of citric acid into $CO_2$ during the calcination process. On the other hand, Figure 7b illustrates that the addition of 12.5 wt% MCC resulted in the formation of smaller and more numerous pores, although the pore distribution remained uneven when compared to the MCC-free sample.

Figure 7d highlights the BOCe sample with 37.5 wt% MCC, showing greater pore density and improved pore uniformity, emphasizing the role of MCC as a natural template in facilitating the formation of structured pores. These observations indicate that higher MCC content enhances both pore distribution and pore size, as confirmed through $N_2$ adsorption-desorption isotherm analysis.

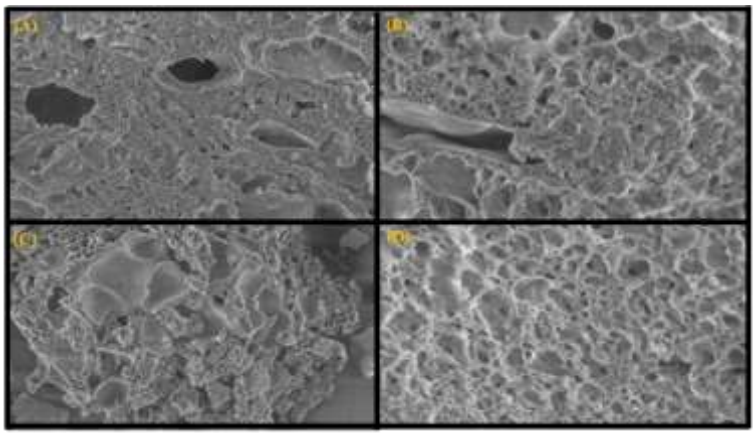

**Figure 7: FESEM images of catalysts a) BOCe, b) BOCe-12,5wt% MCC, c) BOCe-25wt% MCC, and d) BOCe-37,5wt% MCC**

The EDX results, presented in Figure 8, confirm that all BOCe samples, regardless of MCC incorporation, contain Ce, La, and Ni metal elements uniformly distributed throughout the material. The elemental compositions vary depending on MCC content, with detailed percentages summarized in Table 1.

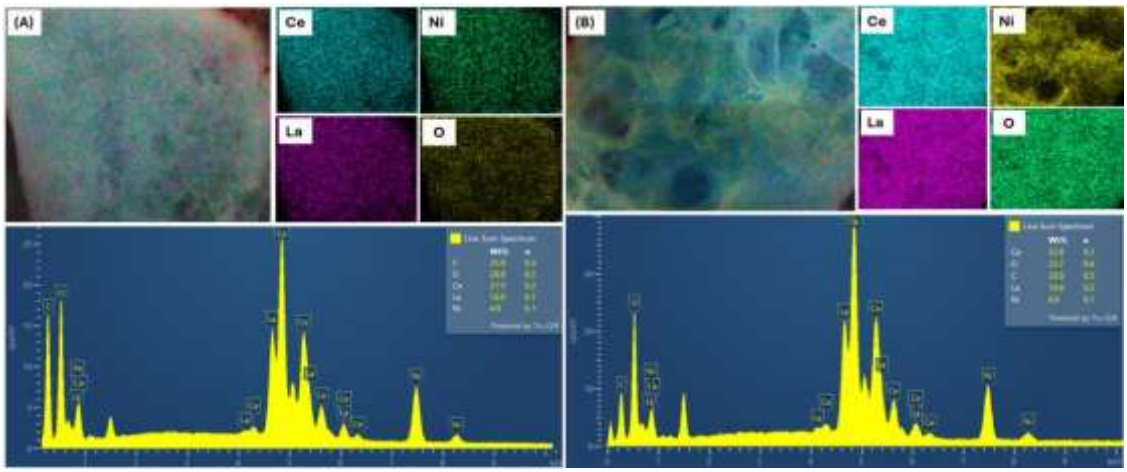

International Journal of Current Science Research and Review
ISSN: 2581-8341
Volume 08 Issue 06 June 2025
DOI: 10.47191/ijcsrr/V8-i6-29, Impact Factor: 8.048
IJCSRR @ 2025
www.ijcsrr.org

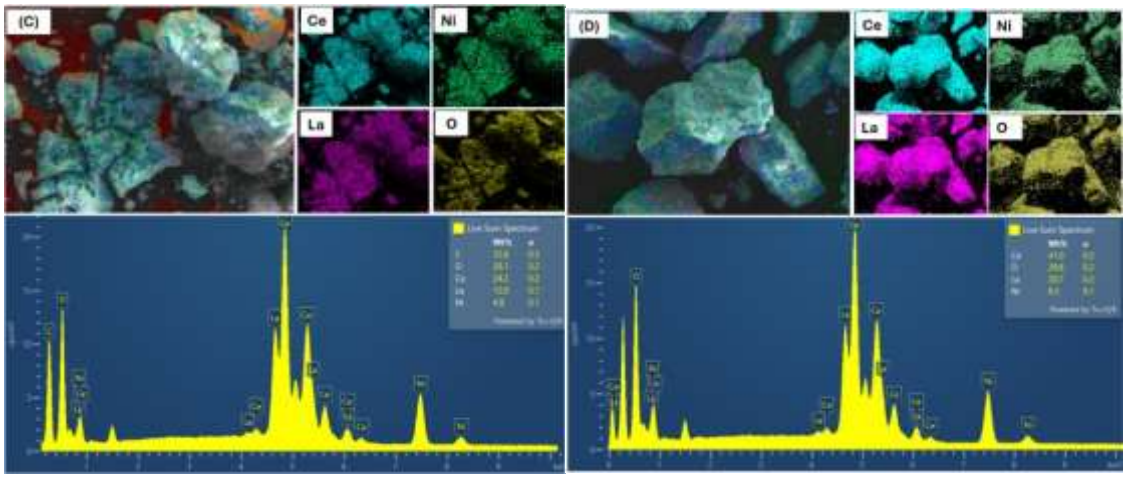


**Figure 8: EDX analysis of catalysts a) BOCe, b) BOCe-12,5wt% MCC, c) BOCe-25wt% MCC, and d) BOCe-37,5wt% MCC**

3.2.5 Nitrogen Adsorption-Desorption Analysis

The $CeO_2$-based oxide catalysts ($CeO_2$-$La_2O_3$-NiO) were synthesized with different proportions of microcrystalline cellulose (MCC). The results of $N_2$ adsorption-desorption isotherms are presented in Figure 9. The results of specific surface area and pore size distribution are presented in Table 1. The isotherms for all catalysts belong to type IV, according to the IUPAC classification, which is characterized by the H3 hysteresis loop, confirming the mesoporous nature of the synthesized materials. Slit-like pores are formed, related to the non-uniform or irregular pore structure. This condition is triggered by the hardening function of MCC when it acts as a template during the synthesis process of the materials(Ruan Y, et al., 2020).

At relative pressures ($P/P_0$) below 0.31, nitrogen initiates pore filling by forming a monolayer within the material. As the relative pressure surpasses 0.41, hysteresis loops emerge, indicating capillary condensation and the gradual adsorption of nitrogen into the mesopores. Table 1 presents the specific surface area data calculated using the BET method. The results reveal that the BOCe-25 wt% MCC sample possesses the largest surface area (52.36 $m^2/g$), followed by BOCe-37.5 wt% MCC (48.25 $m^2/g$), BOCe-12.5 wt% MCC (36.00 $m^2/g$), and pure BOCe (33.41 $m^2/g$). This trend demonstrates that MCC addition significantly enhances surface area, with the optimal concentration being 25 wt% MCC.

Conversely, mesopore volume data (Table 1) indicate a gradual decline in pore volume as MCC concentration increases. The pure BOCe sample features the highest pore volume (0.137 $cm^3/g$), whereas values decrease progressively to 0.077 $cm^3/g$ in BOCe-12.5 wt% MCC, 0.079 $cm^3/g$ in BOCe-25 wt% MCC, and 0.072 $cm^3/g$ in BOCe-37.5 wt% MCC. This reduction suggests that MCC serves as an effective template, facilitating the formation of a highly structured mesoporous network. During calcination, MCC is gradually removed, leaving behind newly developed pores that align with the MCC imprint, thereby yielding a more refined and uniform pore arrangement.

International Journal of Current Science Research and Review
ISSN: 2581-8341
Volume 08 Issue 06 June 2025
DOI: 10.47191/ijcsrr/V8-i6-29, Impact Factor: 8.048
IJCSRR @ 2025
www.ijcsrr.org

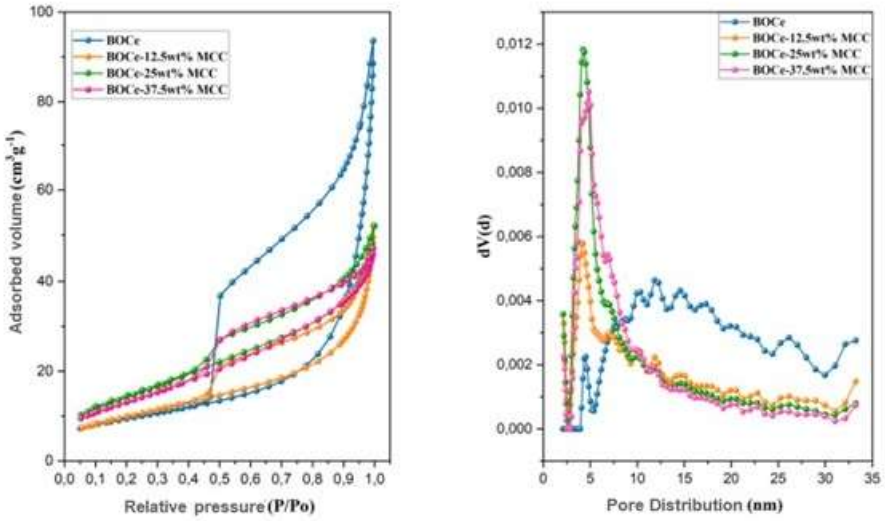


**Figure 9: (a) Isotherm graph and (b) pore distribution of $CeO_2$-based oxide materials ($CeO_2$-$La_2O_3$-NiO)**

Figure 9b presents the pore size distribution of materials incorporating different concentrations of MCC. In BOCe without MCC, the average pore size is 13.68 nm, which notably declines to 6.72 nm in BOCe-12.5 wt% MCC, further decreasing to 5.27 nm in BOCe-25 wt% MCC, before exhibiting a slight increase to 5.39 nm in BOCe-37.5 wt% MCC. This pattern suggests that utilizing MCC as a hard template effectively reduces pore size while improving the uniformity of porosity, with the optimal structure achieved at 25% MCC content.

Overall, MCC functions as a natural templating agent, significantly influencing the mesoporous characteristics of the synthesized material. Its presence facilitates the formation of a structure with smaller, more controlled pores and enhanced uniformity in pore distribution, making it a valuable component in tailoring the physicochemical properties of $CeO_2$-based oxides.

**Table 1: Physicochemical Properties of $CeO_2$-Based Oxides ($CeO_2$-$La_2O_3$-NiO)**

| Sample | $S_{BET}$ ($m^2/g$) | [a]Average Pore Size (nm) | Mesopore Volume ($cm^3/g$) | [b]Elemental Composition | | | |
|---|---|---|---|---|---|---|---|
| | | | | Ce | La | Ni | O |
| BOCe | 33.41 | 13.68 | 0.137 | 33.5 | 16.9 | 7.6 | 42 |
| BOCe-12,5wt% MCC | 36.00 | 6.72 | 0.077 | 41 | 20.8 | 8.6 | 29.6 |
| BOCe-25wt% MCC | 52.36 | 5.27 | 0.079 | 36 | 17.9 | 7.3 | 38.8 |
| BOCe-37,5wt% MCC | 48.25 | 5.39 | 0.072 | 41 | 20.7 | 8.5 | 29.8 |

[a]Average pore size calculated using the BJH desorption method
[b]Elemental composition obtained through EDX analysis.

### 3.3 Deoxygenation Reaction of Waste Cooking Oil Using $CeO_2$-Based Oxide Catalysts

The $CeO_2$-based oxide catalyst that has been successfully synthesized with various concentrations of microcrystalline cellulose (MCC) was used for the deoxygenation reaction process in used cooking oil. A semi-batch reactor type was used, this reactor was equipped with a magnetic stirrer, digital heating mantle, condenser, thermometer, and vacuum system. This deoxygenation reaction involved mixing 10 g of used cooking oil, 1% catalyst in a three-necked round flask. This deoxygenation process was maintained at a temperature of 360°C for 4 hours under a nitrogen atmosphere to prevent oxidation. The final product of this process was a liquid which was then analyzed using Gas Chromatography-Mass Spectrometry (GC-MS) which was used to analyze and identify volatile organic compounds in the sample.

International Journal of Current Science Research and Review
ISSN: 2581-8341
Volume 08 Issue 06 June 2025
DOI: 10.47191/ijcsrr/V8-i6-29, Impact Factor: 8.048
IJCSRR @ 2025
www.ijcsrr.org

As illustrated in Figure 10(a), all catalysts demonstrated exceptional efficiency, achieving 100% conversion of waste cooking oil (Nugraha RE, et al., 2024), previously reported a comparable conversion rate for algae oil when processed with lanthanum-based catalysts. The liquid product yield ranged from 57% to 33%, with the following performance ranking: BOCe > BOCe-12.5 wt% MCC > BOCe-25 wt% MCC > BOCe-37.5 wt% MCC. The highest yield of 57% was obtained using BOCe, likely due to its larger mesoporous volume(Ooi XY, et al., 2024). The mesopore-to-micropore volume ratio in BOCe was significantly higher than in other catalysts, improving reactant accessibility and enhancing product diffusion, thus optimizing mass transfer during deoxygenation.

Figure 10(b) depicts the formation of oxygenated intermediates, such as carboxylic acids, alcohols, and ketones, alongside non-oxygenated compounds, including hydrocarbons, cyclic structures, and aromatic species. Hydrocarbon selectivity was notably high across all catalysts, with BOCe-12.5 wt% MCC yielding the highest hydrocarbon content at 99%, followed by catalysts with MCC concentrations of 0 wt% (98%), 37.5 wt% (94%), and 25 wt% (90%). These findings reinforce the catalytic efficiency of these materials in facilitating deoxygenation. Similar results were reported by Khalit (Aliana-Nasharuddin N, et al., 2019), who documented an 89% hydrocarbon yield using nickel-based catalysts on selected supports. Previous research on bimetallic Ni-Ce catalysts has identified cerium oxide ($CeO_2$) as a crucial component in enhancing catalytic activity. Furthermore, the elevated hydrocarbon yield observed with BOCe can be linked to its larger mesopore diameter (13.68 nm), which is greater than that of other samples with smaller pore sizes. A wider mesopore diameter promotes efficient diffusion of bulky waste cooking oil (WCO) molecules into the active sites of the catalyst, strengthening interactions between the catalyst's acidic sites and WCO, thereby optimizing hydrocarbon selectivity. However, increasing MCC concentration in this study led to a reduction in pore size, restricting reactant accessibility by limiting molecular diffusion to the catalyst surface. Consequently, the structural and dimensional characteristics of catalyst pores play a vital role in determining reactant diffusion efficiency, decomposition kinetics, and product formation within the catalytic matrix, directly influencing the overall performance of the deoxygenation reaction.

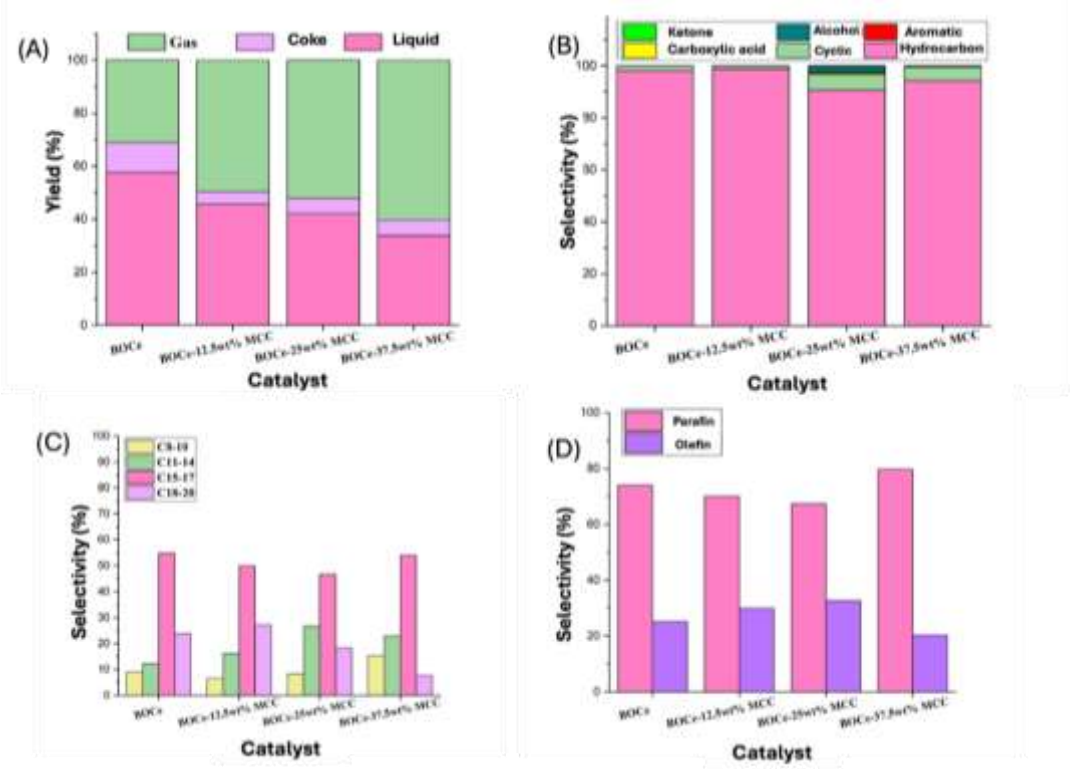


**Figure 10: a) Liquid Yield, b) Selectivity of Product, c) Selectivity of Carbon, and d) Selectivity of Hydrocarbon at Various Catalysts**

International Journal of Current Science Research and Review
ISSN: 2581-8341
Volume 08 Issue 06 June 2025
DOI: 10.47191/ijcsrr/V8-i6-29, Impact Factor: 8.048
IJCSRR @ 2025
www.ijcsrr.org

Analysis of Figure 10(c) reveals that the highest concentration of hydrocarbon fractions falls within the C15–C17 range. This trend is primarily driven by decarboxylation and decarbonylation reactions, which eliminate carbon atoms by releasing $CO_2$ or CO molecules(Baharudin KB, et al., 2019). The presence of C15 and C17 fractions corresponds to the free fatty acid (FFA) components found in waste cooking oil (WCO), predominantly oleic acid (C18:1) and palmitic acid (C16:0), both of which undergo decarboxylation and decarbonylation (DCO/$DCO_2$) transformations(Ooi XY, et al., 2019; Nugraha RE, et al., 2024). As illustrated in Figure 10(d), paraffin formation exceeds olefin production, indicating that decarboxylation is the dominant reaction mechanism(Tamim R, et al., 2024). The selection between decarboxylation (DCX) and decarbonylation (DCN) is influenced by the degree of WCO accessibility to catalytic active sites, which subsequently impacts hydrocarbon formation. In the BOCe catalyst, which features the largest pore diameter (13.68 nm), WCO molecules diffuse more efficiently into active regions, fostering robust acidic interactions that favor alkane hydrocarbon synthesis through decarboxylation. Conversely, the BOCe-37.5 wt% MCC catalyst, characterized by a smaller pore size (5.39 nm, Table 1), primarily generates alkene hydrocarbons via decarbonylation, as restricted diffusion limits reactant access to catalytic sites.

Overall, the reaction mechanism that occurs is an increase in the ratio of paraffin to olefin closely related to hydrogenation, which further forms the distribution and selectivity of hydrocarbons(Zhang L, et al., 2015).

## 4. CONCLUSION

$CeO_2$-based oxide catalysts ($CeO_2$-$La_2O_3$-NiO) were synthesized using microcrystalline cellulose (MCC) as a template. XRD analysis confirmed the presence of stable $CeO_2$ phase in all samples, indicating that increasing MCC content resulted in smaller crystallite sizes. The incorporation of MCC also increased the surface area of the product material and its pore size, which contributed greatly to the enhancement of catalytic performance. Of the tested materials, BOCe-12.5 wt% MCC showed excellent efficiency in converting hazardous and less useful waste cooking oil (WCO) into environmentally friendly biofuel. The catalyst achieved a complete conversion rate of 100%, an excellent hydrocarbon selectivity yield approaching 99%, and a final liquid product yield of 45%. This superior catalyst performance can be attributed to the synergistic interaction between lanthanum (La), nickel (Ni), and cerium (Ce), which makes it a promising candidate material for sustainable green biofuel production.

## ACKNOWLEDGMENTS

This research was fully supported by the Energy and Environment Laboratory at ITS and the Materials and Energy Laboratory of the ITS Department of Chemistry. The authors would also like to extend their gratitude to all parties who contributed to and supported the completion of this study.

## REFERENCES

1. Adedoyin FF, Alola AA, Bekun FV. The alternative energy utilization and common regional trade outlook in EU-27: Evidence from common correlated effects. Renew Sustain Energy Rev 2021;145:111092. https://doi.org/10.1016/j.rser.2021.111092.
2. Aliana-Nasharuddin N, Asikin-Mijan N, Abdulkareem-Alsultan G, Saiman MI, Alharthi FA, Alghamdi AA, et al. Production of green diesel from catalytic deoxygenation of chicken fat oil over a series binary metal oxide-supported MWCNTs. RSC Adv 2019;10:626–42. https://doi.org/10.1039/c9ra08409f..
3. Baharudin KB, Taufiq-Yap YH, Hunns J, Isaacs M, Wilson K, Derawi D. Mesoporous NiO/Al-SBA-15 catalysts for solvent-free deoxygenation of palm fatty acid distillate. Microporous Mesoporous Mater 2019;276:13–22. https://doi.org/10.1016/j.micromeso.2018.09.014..
4. Barbosa KKF, Aristizábal-Giraldo D, Osorio-Guillén JM, Acuña JJS, Ferreira FF. Green-chemistry synthesis and optical properties of lead-free Cs 2 AgSbCl 6 double perovskite by a mechanochemical method . RSC Mechanochemistry 2024;1:69–77. https://doi.org/10.1039/d3mr00024a..
5. Bian Z, Wang Z, Jiang B, Hongmanorom P, Zhong W, Kawi S. A review on perovskite catalysts for reforming of methane to hydrogen production. Renew Sustain Energy Rev 2020;134:110291. https://doi.org/10.1016/j.rser.2020.110291..
6. Çoban Özkan D, Türk A, Çelik E. Synthesis and characterizations of sol–gel derived $LaFeO_3$ perovskite powders. J Mater Sci Mater Electron 2020;31:22789–809. https://doi.org/10.1007/s10854-020-04803-8.

International Journal of Current Science Research and Review
ISSN: 2581-8341
Volume 08 Issue 06 June 2025
DOI: 10.47191/ijcsrr/V8-i6-29, Impact Factor: 8.048
IJCSRR @ 2025
www.ijcsrr.org

7. Hosseinzadeh-Bandbafha H, Li C, Chen X, Peng W, Aghbashlo M, Lam SS, et al. Managing the hazardous waste cooking oil by conversion into bioenergy through the application of waste-derived green catalysts: A review. J Hazard Mater 2022;424:127636. https://doi.org/10.1016/j.jhazmat.2021.127636.
8. Li X, Fu H, Shao S, Cai Y. Synthesis of hierarchical HZSM-5 utilizing natural cellulose as templates for promoted production of aromatic hydrocarbons in the catalytic pyrolysis of biomass. Fuel Process Technol 2023;248:107815. https://doi.org/10.1016/j.fuproc.2023.107815.
9. Loizides MI, Loizidou XI, Orthodoxou DL, Petsa D. Circular bioeconomy in action: Collection and recycling of domestic used cooking oil through a social, reverse logistics system. Recycling 2019;4. https://doi.org/10.3390/recycling4020016.
10. Nugraha RE, Purnomo H, Aziz A, Holilah H, Bahruji H, Asikin-Mijan N, et al. The mechanism of oleic acid deoxygenation to green diesel hydrocarbon using porous aluminosilicate catalysts. South African J Chem Eng 2024;49:122–35. https://doi.org/10.1016/j.sajce.2024.04.009.
11. Ooi XY, Gao W, Ong HC, Lee HV, Juan JC, Chen WH, et al. Overview on catalytic deoxygenation for biofuel synthesis using metal oxide supported catalysts. Renew Sustain Energy Rev 2019;112:834–52. https://doi.org/10.1016/j.rser.2019.06.031.
12. Pham LKH, Tran TTV, Kongparakul S, Reubroycharoen P, Karnjanakom S, Guan G, et al. Formation and activity of activated carbon supported $Ni_2P$ catalysts for atmospheric deoxygenation of waste cooking oil. Fuel Process Technol 2019;185:117–25. https://doi.org/10.1016/j.fuproc.2018.12.009..
13. Qian M, Zhao Y, Huo E, Wang C, Zhang X, Lin X, et al. Improving catalytic production of aromatic hydrocarbons with a mesoporous ZSM-5 modified with nanocellulose as a green template. J Anal Appl Pyrolysis 2022;166:105624. https://doi.org/10.1016/j.jaap.2022.105624.
14. Ruan Y, Zhao Y, Lu Y, Guo D, Zhao Y, Wang S, et al. Mesoporous $LaAl_{0.25}Ni_{0.75}O_3$ perovskite catalyst using SBA-15 as templating agent for methane dry reforming. Microporous Mesoporous Mater 2020;303:110278. https://doi.org/10.1016/j.micromeso.2020.110278.
15. Sagar T V., Sreelatha N, Hanmant G, Surendar M, Lingaiah N, Rama Rao KS, et al. Influence of method of preparation on the activity of La-Ni-Ce mixed oxide catalysts for dry reforming of methane. RSC Adv 2014;4:50226–32. https://doi.org/10.1039/c4ra07098d.
16. Tamim R, Prasetyoko D, Jovita S, Ni'mah YL, Nugraha RE, Holilah H, et al. Low temperature pyrolysis of waste cooking oil using marble waste for bio-jet fuel production. Renew Energy 2024;232:121135. https://doi.org/10.1016/j.renene.2024.121135.
17. Tsiotsias AI, Hafeez S, Charisiou ND, Al-Salem SM, Manos G, Constantinou A, et al. Selective catalytic deoxygenation of palm oil to produce green diesel over Ni catalysts supported on $ZrO_2$ and $CeO_2$–$ZrO_2$: Experimental and process simulation modelling studies. Renew Energy 2023;206:582–96. https://doi.org/10.1016/j.renene.2023.02.038.
18. Wang L, Zhao N, Yin X, Wang W, Zhao Y, Zheng Z, et al. Highlights on the key roles of interfaces between $CeO_2$-based oxide and perovskite ($LaMnO_3$/$LaFeO_3$) in creating active oxygen species for soot oxidation. Fuel 2024;356:129444. https://doi.org/10.1016/j.fuel.2023.129444.
19. Xu M, Shi Z, Zhu X, Lai Y, Xia A, Huang Y, et al. Ex-situ catalytic upgrading of biomass pyrolysis volatiles over thermal-decomposition products of spent lithium-ion batteries for bio-oil deoxygenation and hydrogen-rich syngas production. Int J Hydrogen Energy 2024;52:83–96.https://doi.org/10.1016/j.ijhydene.2023.07.286.
20. Ye C, Wang R, Wang H, Jiang F. The high photocatalytic efficiency and stability of $LaNiO_3$/g-$C_3N_4$ heterojunction nanocomposites for photocatalytic water splitting to hydrogen. BMC Chem 2020;14:1–13. https://doi.org/10.1186/s13065-020-00719-w.
21. Zhang L, Gu L, Ringler P, Smith S, Rushton PJ, Shen QJ. Three WRKY transcription factors additively repress abscisic acid and gibberellin signaling in aleurone cells. Plant Sci 2015;236:214–22. https://doi.org/10.1016/j.plantsci.2015.04.014.

***Cite this Article: Rosyidah, A., Octora, R.W.P. (2025). Conversion of Waste Cooking Oil into Biofuel through $CeO_2$-Based Oxide Catalysts ($CeO_2$-$La_2O_3$-NiO). International Journal of Current Science Research and Review, 8(6), pp. 2958-2971. DOI: https://doi.org/10.47191/ijcsrr/V8-i6-29***